Noninvasive Molecular Imaging to Detect Transgene Expression of Lentiviral Vector in Nonhuman Primates

William E. Sander[1], Mark E. Metzger[1], Kouki Morizono[2], Aylin Bonifacino[1], Scott R. Penzak[3], Yi-Ming Xie[2], Irvin S.Y. Chen[2], Jeffrey Bacon[4], Stephen G. Sestrich[4], Lawrence P. Szajek[4], and Robert E. Donahue[1]

[1]Hematology Branch, National Heart, Lung, and Blood Institute, Rockville, Maryland; [2]AIDS Institute, UCLA School of Medicine, Los Angeles, California; [3]Clinical Pharmacokinetics Research Laboratory, Pharmacy Department, NIH Clinical Center, Bethesda, Maryland; and [4]PET Imaging Section, NIH Clinical Center, Bethesda, Maryland

Noninvasive imaging of a reporter gene is a new and promising technique to quantify transgene expression after gene therapy. This study was performed to demonstrate visualization of lentiviral-marked cells by PET. **Methods:** We transduced nonhuman primate $CD34^+$ hematopoietic cells with a lentiviral vector expressing a PET reporter gene, the mutant viral herpes simplex virus type 1–thymidine kinase (HSV1-sr39tk) gene. 1-(2-Fluoro-2-deoxy-β-D-arabinofuranosyl)-^{76}Br-5-bromouracil (^{76}Br-FBAU) was used as the substrate for the viral tk enzyme. Upon phosphorylation, ^{76}Br-FBAU was retained by cells and imaged by PET. The long half-life of ^{76}Br, 16.2 h, permitted us to perform extended pharmacokinetic and imaging studies. **Results:** ^{76}Br-FBAU was retained in vascular tissues of the animals with transplanted tk lentiviral vector–transduced $CD34^+$ cells. Elimination of ^{76}Br-FBAU was through renal and hepatic excretion. **Conclusion:** Noninvasive molecular imaging using PET will help us, in the future, to define the contribution and distribution of cells and their progeny to tissue repair and development.

Key Words: ^{76}Br-FBAU; gene therapy; PET; nonhuman primates; molecular imaging

J Nucl Med 2006; 47:1212–1219

One question currently plaguing stem cell research is how to determine whether a cell of a defined phenotype can contribute to tissue development and repair in living organisms. Numerous approaches have been taken to address this question, but most involve in vitro studies that isolate the cells of a particular origin and, with a variety of cytokine cocktails, allow them to differentiate to other tissue types. To date, few studies have been performed in vivo to evaluate how phenotypically defined cells contribute to tissue development and repair. Most studies have required invasive procedures such as organ removal or biopsy. To better define whether a cell and its progeny can contribute to tissue engraftment and repair, long-term follow-up studies using noninvasive approaches are needed.

Evaluation of gene expression has been restricted primarily to tissue samples collected by biopsy or necropsy. Biopsy procedures are limited by tissue access and level of marking, and necropsy is a terminal procedure. Reporter genes such as luciferase have been applied in vivo to localize gene expression using sensitive video imaging (*1*), and novel approaches using fluorescent semiconductor nanocrystals (quantum dots) are being pursued (*2*). Such imaging techniques, however, are limited by tissue depth, tomographic resolution, and an inability to quantify gene expression. Other approaches for evaluating cellular distribution include the direct radiolabeling of cells and, recently, the loading of cells with paramagnetic particles for MRI (*3*). These approaches, however, are limited by their inability to effectively evaluate cellular progeny and by their potential for perturbing normal cellular distribution by in vitro manipulation.

Still other approaches have been developed involving the use of gene transfer and PET reporter gene technology. These approaches take advantage of receptor–ligand or enzyme–substrate interactions using radiolabeled ligand or substrate, respectively. One approach involves gene transfer of the herpes simplex virus type 1–thymidine kinase (HSV1-tk) gene. The success of this approach is based on the HSV1-tk enzyme, and not the endogenous mammalian tk, to preferentially phosphorylate acycloguanosine and uracil derivatives that have been tagged with a positron emitter. The phosphorylated products cannot leave the target cell, and gene expression is quantified by noninvasive PET. Initial studies on small-animal models have proven quite successful in imaging cells transfected with plasmid (*4*), adenovirus (*5*), herpes virus (*6*), and murine retroviral vector (*7*) containing the HSV1-tk gene. Tumor masses as small as 6 mm^3 that contain tumor cells transduced with a bicistronic vector could be resolved in nude mice using

Received Dec. 20, 2005; revision accepted Apr. 26, 2006.
For correspondence or reprints contact: Robert E. Donahue, VMD, Hematology Branch, NHLBI, 5 Research Ct., Rockville, MD 20850.
E-mail: donahuer@nhlbi.nih.gov
Guest Editor: Sanjiv Gambhir

PET (*4*). In a human study on patients with glioblastoma, a site-directed intratumoral infusion of a cationic liposomal vector carrying an HSV1-tk plasmid was used to visualize the tumor site by PET (*8*).

In extending these approaches to nonhuman primate models, several limitations have to be considered. These include selection of a HSV1-tk–containing vector capable of targeting the chosen cell type and expressing the gene of interest; selection of a positron-emitting isotope and substrate having an energy and half-life that allow adequate PET imaging and having a pharmacokinetic distribution that results in low background activity in the evaluated tissues; selection of instrumentation sufficiently sensitive for spatial and volumetric resolution of a critical mass of gene-expressing cells; and selection of an animal model tolerant of the foreign HSV1-tk so that long-term follow-up PET studies can be performed. To achieve these aims, we constructed 2 self-inactivating (SIN) lentiviral vectors. The first contained the mutant HSV1-sr39tk gene (SINcppt2sr39tk2), an excellent PET reporter (*9*). The second vector contained an optical reporter gene, enhanced green fluorescent protein (EGFP) (SIN18cpptRhMLV-E). Both vectors were used to cotransduce nonhuman primate immunoselected $CD34^+$ cells isolated from cytokine-mobilized peripheral blood (PB) under serum-free conditions and transplanted into irradiated rhesus macaques (*10*), which subsequently became tolerant of the foreign gene product on reconstitution (*11*). The radioligand selected, 1-(2-fluoro-2-deoxy-β-D-arabinofuranosyl)-^{76}Br-5-bromouracil (^{76}Br-FBAU), took advantage of the extended half-life of the positron emissions of ^{76}Br, permitted evaluation of the pharmacokinetics of ^{76}Br-FBAU, and allowed us to perform extensive PET imaging. The use of EGFP also permitted us to optically evaluate EGFP gene expression over time in circulating granulocytes, monocytes, lymphocytes, platelets, and red blood cells using flow cytometry. These techniques provided us the opportunity to follow the distribution of transduced cells using noninvasive, real-time imaging. In this study, we localized transduced $CD34^+$ cells and their progeny using PET in a nonhuman primate transplant model and studied the pharmacokinetic properties of ^{76}Br-FBAU.

MATERIALS AND METHODS

Isolation, Transduction, and Transplantation of Immunoselected $CD34^+$ Cells

This study used blood group B rhesus macaques free of specific pathogens (serologically negative for simian T-lymphotropic virus, simian immunodeficiency virus, simian retrovirus, and herpesvirus B). Hematopoietic progenitor and stem cells were mobilized into the PB by subcutaneous injection of granulocyte colony-stimulating factor (10 μg/kg/d) and stem cell factor (100 μg/kg/d) (both cytokines were kindly provided by Amgen, Inc.) for 5 consecutive days using a protocol approved by the Animal Care and Use Committee of the National Heart, Lung, and Blood Institute. On the fifth day, leukapheresis was performed under general anesthesia, using procedures previously described (*10*). Blood was drawn through a surgically placed central line catheter by a CS-3000 Plus blood cell separator (Baxter) specially fitted with a small-volume, shunt chamber so that animals weighing 5 kg could undergo leukapheresis. Peripheral blood mononuclear cells were collected in the small-volume chamber, and packed red blood cells and plasma were returned to the animal through a second catheter placed in a peripheral vein. The product of the apheresis was enriched for $CD34^+$ cells by immunomagnetic selection using a biotinylated $CD34^+$ clone 12.8 monoclonal antibody (originally obtained from CellPro, Inc.), Streptavidin MicroBeads (Miltenyi Biotec), LS Column (Miltenyi Biotec), and VarioMACS magnet (Miltenyi Biotec), using techniques previously described (*10*). Immunoselected $CD34^+$ cells (5×10^7, having a purity of 90% or better based on flow cytometry) were then transduced twice over a 48-h period with both the SINcppt2sr39tk2 vector and the SIN18cpptRhMLV-E, using an equivalent amount of vector based on p24 levels. The SIN18cpptRhMLV-E vector has previously been described (*11,12*). SINcppt2srtk2 was constructed by exchanging the EGFP gene of the SIN18cpptRhMLV-E with the HSV1-tk mutant SR39 gene (*13*). Vesicular stomatitis virus G protein (VSV-G)-pseudotyped lentivirus vectors were produced by calcium phosphate transfection of 293T cells. 293T cells (2×10^7) were transfected with 12.5 μg of pCMVdR8.2DVPR (*14*), 12.5 μg of lentivirus vectors, and 5 μg of VSV-G expression vector (*15*). 293T cells were cultured in Dulbecco's modified Eagle medium with 10% fetal bovine serum, 100 U of penicillin per milliliter, and 100 μg of streptomycin per milliliter.

Supernatants were collected on days 2 and 3 after transfection and were filtered through a 0.22-μm-pore filter. The vector concentration was achieved by ultracentrifugation at 40,000*g* for 90 min at 4°C. The pellet was resuspended in phosphate-buffered saline. The concentration of p24 (HIV CA protein) in the concenrated lentivirus vectors was determined by ELISA (Beckman Coulter). The concentration of p24 was 44.1 μg/mL for SIN18cpptRhMLV-E and 27.3 μg/mL for SINcppt2sr39tk2. The EGFP vector was titrated on 293T cells. The titer of the concentrated vector was 1.5×10^9/mL. The $CD34^+$ cells were transduced by the EGFP-expressing vector at the multiplicity of infection of 10. The function of SINcppt2sr39tk2 was confirmed by cytotoxic assay using ganciclovir (*16*). The $CD34^+$ cells were transduced with the tk-expressing vector using the same concentration of p24 as for the EGFP expressing virus. All transductions were performed in serum-free defined medium (X-Vivo 10; Cambrex) with no additional cytokines. One day after the leukapheresis procedure, the animal was irradiated with 500 cGy of total-body irradiation daily for 2 consecutive days (a total dose of 1,000 cGy over 2 d). The day after the last dose of irradiation, the transduced cells (3×10^7 for 2RC003 and 2×10^7 for CJ2R) were reinfused via a central venous catheter. Approximately 30% of cells expressed EGFP on the day of reinfusion.

Cyclotron Production of ^{76}Br

^{76}Br (half-life, 16.2 h) was prepared at the National Institutes of Health (NIH) cyclotron facility using natural arsenic metal targets and the nuclear reaction As(^{3}He,2n)^{76}Br. Dried ^{76}Br-NH_4Br was obtained after wet-chemical distillation of the irradiated target material (*17*).

Radiosynthesis of ^{76}Br-FBAU

^{76}Br-FBAU was prepared according to methods described in the literature (*17*). Briefly, to dry ^{76}Br-NH_4Br were added

1-(2′-fluoro-2′-deoxy-β-D-arabinofuranosyl)-5-trimethyl-stannyluracil (100 μg) and water (30 μL), followed by peracetic acid (30 μL, 0.3% v/v in acetic acid). The solution was stirred in a vortex mixer and allowed to stand at room temperature for 20 min. To the reaction mixture was added a 0.1 mol/L concentration of NaH_2PO_4 (40 μL), and the entire solution was injected onto a Supelcosil LC-18-S (4.6 × 250 mm) analytic high-performance liquid chromatography column (Supelco) eluting with phosphate buffer (pH 5, 0.05 mol/L) and 9% ethyl alcohol at 1 mL/min. The wavelength for ultraviolet detection was 278 nm. The product eluting at 9 min was collected and passed through a 0.2-μm sterile filter. The specific activity of ^{76}Br-FBAU was 406,408 ± 155,400 GBq/mmol (10,984 ± 4,200 Ci/mmol) as determined by reinjection of the formulated compound onto an identical high-performance liquid chromatography column.

PET Procedure

The animals were sedated with a combination of tiletamine hydrochloride and zolazepam hydrochloride (Telazol; Fort Dodge Animal Health) (4 mg/kg), ketamine (4 mg/kg), and atropine (0.1 mg/kg) by intramuscular injection, and anesthesia was maintained with isoflurane (1%–2%) by inhalation. A catheter with a 3-way stopcock attachment was placed in each saphenous vein. Seventy-four megabecquerels of ^{76}Br-FBAU were injected through 1 catheter over a period of about 30 s. Serial blood samples (0.5 mL) were collected through the opposite catheter (at 1, 2, 3, 4, 5, 6, 8, 10, 12, 15, 20, 25, 30, 35, 40, 50, 60, 75, 90, 105, 120, 150, 180, 210, and 240 min), processed, and stored at −80°C until analyzed for the presence of ^{76}Br-FBAU. For all time points, 0.1 mL of whole-blood samples were counted for 2 min in a COBRA model 5003 γ-counter (Packard Instrument Co.) using an energy window of 400–1,200 keV and expressed in activity concentrations. The remaining collected blood was spun on a centrifuge. Pharmacokinetic parameter values for ^{76}Br-FBAU were determined using compartmental analysis. Experimental whole-blood concentration–time profiles were fitted to a 2-compartment pharmacokinetic model with intravenous bolus and linear first-order elimination from the central compartment using the WinNonlin Professional computer program (version 3.2; Pharsight). Model selection was guided by visual inspection of the distribution of the residuals, the Akaike information criterion, the sums of the squared residuals, and the predicted-versus-measured data (*18*). The model fit the observed data well, with a mean r^2 value of 0.988 (range, 0.975–0.997) for whole-blood curves and 0.988 (range, 0.976–0.997) for plasma curves. The regression lines through the plot of observed versus estimated concentrations did not differ from the line of identity, and no bias was observed. Peak concentrations for whole blood were determined as model-estimated concentrations immediately after bolus administration, and values for area under the concentration–time curve from zero to infinity were calculated from estimated concentration–time profiles using the trapezoidal rule with extrapolation to infinity and standard techniques. The secondary pharmacokinetic parameter values derived from model estimates included distribution half-life (α-phase half-life), terminal elimination half-life (β-phase half-life), and whole-blood clearance; values were determined using standard methods. The pharmacokinetic parameter values for ^{76}Br-FBAU for monkey CJ2R at various times after cell transplantation were compared with the pretransplantation values using a 2-tailed, unpaired Student *t* test (Excel 2003; Microsoft). Correction for multiple comparisons was implemented such that a *P* value of less than 0.0167 was accepted as statistically significant. Pharmacokinetic parameter values for ^{76}Br-FBAU for monkey 2RC003 were compared using the same methods.

The PET procedure followed radiation safety guidelines approved by the NIH. Because of the 16.2-h half-life of ^{76}Br, the animal was housed in an isolated room for 7 d after the PET scan, and the animal's waste, cage, and floor area were monitored daily with a Geiger counter and a final smear survey. All waste was treated as radioactive, with appropriate precautions and disposal techniques. After 7 d, the animal was returned to the home facility.

PET images were taken before transplantation and 1, 3, 6, 12, and 14 mo after transplantation. In addition, blood samples were analyzed regularly for EGFP transgene expression by flow cytometry using a Cytometrics FC 500 MPL flow cytometer (Beckman Coulter). Cell populations were gated on the basis of forward and side scatter. Real-time DNA polymerase chain reaction (PCR) analysis was performed on DNA isolated by a QIAamp DNA blood mini kit (QIAGEN) after treatment of whole blood with ammonium chloride, potassium carbonate (ACK), lysing buffer to remove red blood cells. The vector copy number and cell number in the DNA isolate were quantified by using a SYBRgreen real-time PCR kit (QIAGEN) and an ABI PRISM 7700 sequence detector (PerkinElmer). The primers were tk-X (acaaaagccacggaagtcc) and tk-Y (agttgcgtggtggtggttt) for tk and BG212 (tgcttacatttgcttctgacacaac) and BGR (tccacgttcaccttgccc) for β-globin.

The limit of detection for the SYBRgreen real-time PCR analysis was approximately 10 in 10^5 cells based on a standard curve reference (data not shown). The flow cytometric and SYBRgreen real-time PCR results were the same when EGFP expression levels were examined. Limits in cell number and current technology prevented us from determining the percentage of $CD34^+$ cells expressing tk at the time of reinfusion, the percentage of cells coexpressing EGFP and tk in the circulation, and the level of expression of tk at the RNA and protein level.

Images were generated by the PET department in the clinical center of the NIH on a Digital Imaging and Communications in Medicine system and further processed using MedX (Medical Numerics) on a Linux operating system. The images gathered for the 120- to 240-min duration of the PET scan were used because they illustrated the distribution of ^{76}Br-FBAU throughout the subject. The contrast of all images was adjusted to better elucidate the positive radiation signal in the subject. Areas were drawn around the critical sections of the subject: liver, kidneys, bladder, brain, and extremities. From these areas, MedX could give the exact area encircled, the average concentration of the radiation, and the SD. This information was recorded using Excel. The pixel intensities of fixed areas of all 4 limbs on the 120- to 240-min summed images were averaged and standardized to the bladder (renal excretion is the primary route of elimination) to give a measurable percentage of gene expression. Extremity mean image intensities in monkeys CJ2R and 2RC003, as a percentage of bladder mean intensity, were compared over time using the Student *t* test; again, a *P* value of less than 0.0167 was accepted as statistically significant.

Data on whole blood collected at various times throughout the PET scan were used to create the pharmacokinetic graphs. Graphs of simple time versus radiation concentration were plotted for the test subjects, monkeys CJ2R and 2RC003. The radiation concentrations were averaged for 6 control animals at each time point and graphed. The 95% confidence interval was calculated and added as an error bar to the control animal graph.

RESULTS

Transplantation of Transduced CD34$^+$ Cells

Immunoselected CD34$^+$ cells (5×10^7) were isolated by immunoselection from the leukapheresis product of animals mobilized with granulocyte colony-stimulating factor and stem cell factor for 5 d. The cells were cotransduced with human SIN lentiviral vectors expressing EGFP and a comparable amount of HSV1-tk vector based on p24 determination so that we could monitor gene expression with both flow cytometry and PET. The multiplicity of infection was 10 for the EGFP vector and estimated to be 1–2 for the tk-containing vector. EGFP expression was followed in circulating granulocytes, lymphocytes, monocytes, red blood cells, and platelets for more than 1 y in both animals (Figs. 1 and 2). One of the animals (CJ2R) has had consistent EGFP gene expression at the 1% level or less (Fig. 1), and the second animal (2RC003) has had expression at the 5% level or less in all lineages (Fig. 2). Quantitation of HSV1-tk copy number and β-globin number was calculated on the basis of HSV1-tk copy number/cell number using a real-time PCR curve for each standard and primer combination. We tested samples at approximately 3 mo, 6 mo, and 1 y. For monkey 2RC003 the HSV1-tk copy numbers per 1,000 cells were 1.96, 0.93, and 0.83 at 3 mo, 6 mo, and 1 y, respectively, and for monkey CJ2R the copy number was undetectable at all time points.

Pharmacokinetics of ^{76}Br-FBAU

The mean (±SD) whole-blood ^{76}Br-FBAU concentration–time curve was determined for 6 healthy control animals (Fig. 3). ^{76}Br-FBAU whole-blood concentrations declined in 2 phases and fit a 2-compartment pharmacokinetic model exceedingly well. The mean α- and β-phase half-lives in whole blood were 2.60 ± 0.70 min and 107.80 ± 31.92 min, respectively, for the control animals.

After characterizing baseline pharmacokinetic behavior, we acquired data for the 2 monkeys that received the transplant. Figure 3 illustrates elimination of ^{76}Br-FBAU in the 2 monkeys through analysis of blood samples throughout the 240-min PET scan. The figure focuses on the terminal elimination (β-phase half-life) portion of the concentration–time curve to demonstrate the differences in blood retention levels between monkey 2RC003 and monkey CJ2R during PET. There were no differences between groups and the area under the curve for the distribution (α) phase of the concentration–time curve. In contrast, the median of the area under the curve for the terminal elimination (β) phase was 18% higher for monkey CJ2R and 64% higher for monkey 2RC003 than for the controls. Monkey 2RC003 consistently had greater retention of ^{76}Br-FBAU than did monkey CJ2R or the controls (Fig. 3). The average concentration for monkey 2RC003 was significantly greater 3 mo after cell transplantation than before transplantation (36,681 vs. 14,622 Bq/mL, $P = 0.0061$). Differences between average concentrations before transplantation and at months 6 and 14 did not reach statistical significance, although several trends were observed (P values for 6 and 14 mo vs. the pretransplantation value were 0.061 and 0.129, respectively). A limited sample size most likely precluded our ability to achieve statistical significance among these comparisons. Conversely, for monkey CJ2R, differences in average concentrations before and after transplantation were not statistically significant, nor were any trends noted (P values ranged from 0.518 to 0.982).

PET Image Analysis

Body regions were evaluated using MedX software, which analyzed the pixel intensity of images generated at the 120- to 240-min time points. Pixel intensity for the extremities (right and left leg and arm) using a fixed volume were standardized to bladder intensity (^{76}Br-FBAU is excreted predominantly through the renal system), averaged, and the SD was calculated (Fig. 4). Ratios of extremity mean intensity (normalized to bladder mean intensity) on images

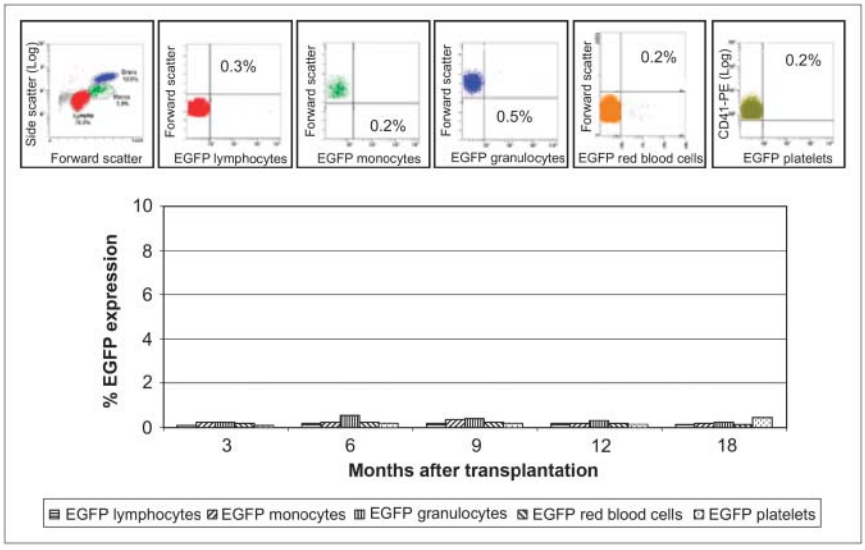

FIGURE 1. Flow cytometry data for monkey CJ2R. Top section contains dot plots for gated cell types: granulocytes, monocytes, lymphocytes, red blood cells, and CD41$^+$ platelets and their respective percentages of prevalence of EGFP in blood at 14 mo. Bottom section contains bar graph of percentages of EGFP in different blood cell types over period of 1.5 y.

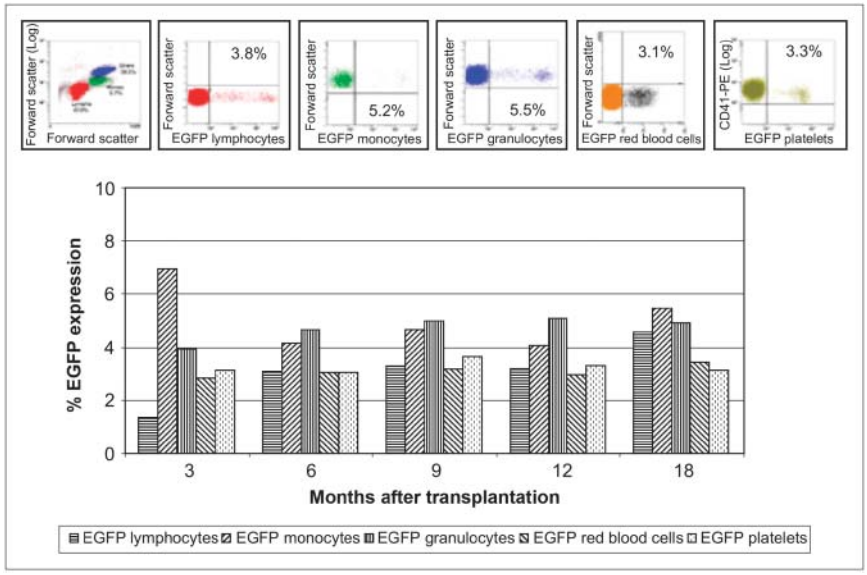

FIGURE 2. Flow cytometry data for monkey 2RC003. Top section contains dot plots for gated cell types: granulocytes, monocytes, lymphocytes, red blood cells, and CD41$^+$ platelets and their respective percentages of prevalence of EGFP in blood at 14 mo. Bottom section contains bar graph of percentages of EGFP in different blood cell types over period of 1.5 y.

obtained at 3, 6, and 14 mo after transplantation were compared with the ratios before transplantation for monkey CJ2R. Intensities at 3 mo ($P = 0.92$), 6 mo ($P = 0.01$), and 14 mo ($P = 0.29$) did not differ from pretransplantation values, with statistical significance being achieved when the P value was less than 0.00625 (0.05/8) (Fig. 4). Conversely, for monkey 2RC003, intensities at all time points (3, 6, and 14 mo) were significantly greater than the pretransplantation values ($P < 0.00000003$) (Fig. 4). Upon comparing monkeys CJ2R and 2RC003 with the controls (Fig. 4), we

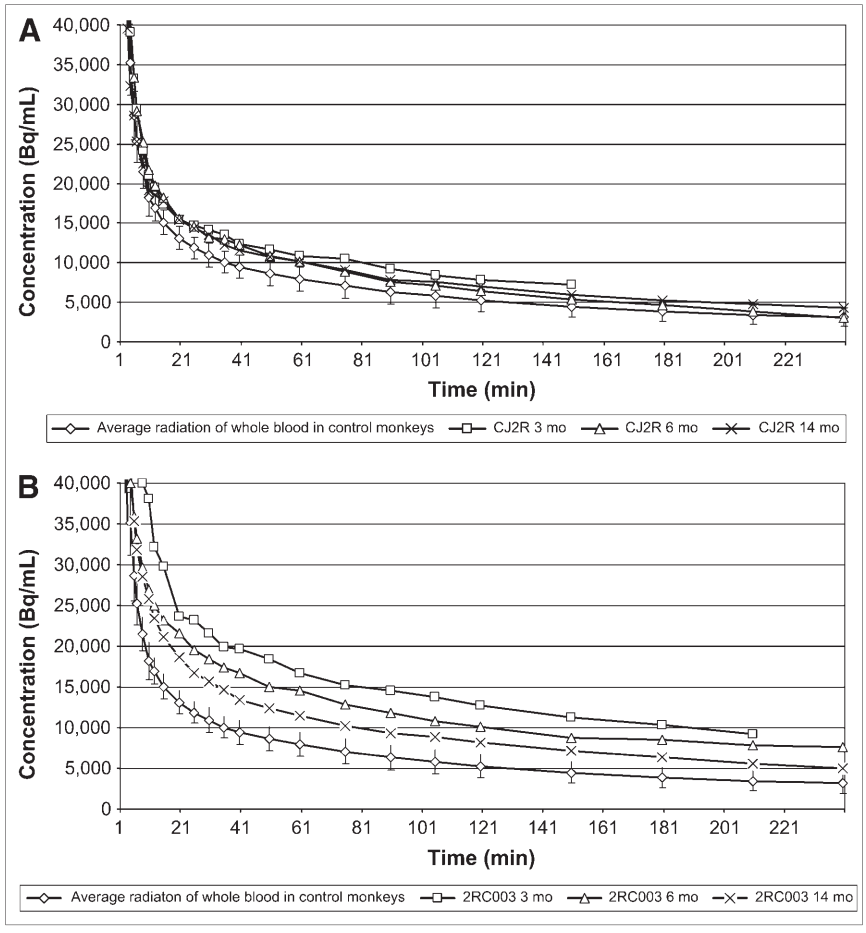

FIGURE 3. Two profiles of concentration vs. time showing distribution and elimination of ^{76}Br-FBAU in monkeys CJ2R (A) and 2RC003 (B) at 3, 6, and 14 mo. Also shown is average radioactivity of whole blood for control monkeys, with 95% confidence bars, in becquerels per milliliter of blood taken at time points between 1 and 240 min.

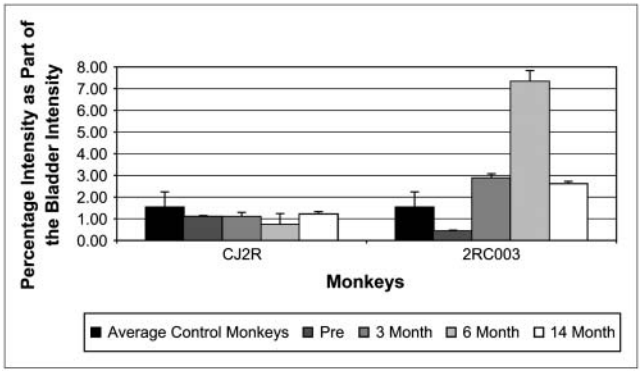

FIGURE 4. Bar graph of average radioactive intensity for extremities as percentage of bladder radioactive intensity for control monkeys (n = 8). Monkeys CJ2R and 2RC003 were graphed in same way at 4 time points: 1 before and 3 after transplantation.

found no significant differences between monkey CJ2R and the controls at 3 mo ($P = 0.14$), 6 mo ($P = 0.02$), or 14 mo ($P = 0.27$); a P value of less than 0.01 was needed, because 7 t tests were performed (0.05/7 = 0.007). Monkey 2RC003, however, differed significantly at 3 mo ($P = 0.001$), 6 mo ($P = 0.000000004$), and 14 mo ($P = 0.005$). Most notable was the difference in the averaged 120- and 240-min images between monkeys CJ2R and 2RC003 (Fig. 5) after the intravenous administration of 74 MBq of ^{76}Br-FBAU. The images were colored similarly using MedX to contrast pixel intensity. The most radioactive organ systems were those involved in elimination, that is, the urinary bladder, kidneys, and liver, with the least radioactive organ being the brain (^{76}Br-FBAU did not appear to cross the blood–brain barrier). All acquired images for monkey 2RC003 demonstrated that radiolabel was retained throughout the animal, outlining predominantly the vasculature and spleen, with the uptake being reticulated and patchy.

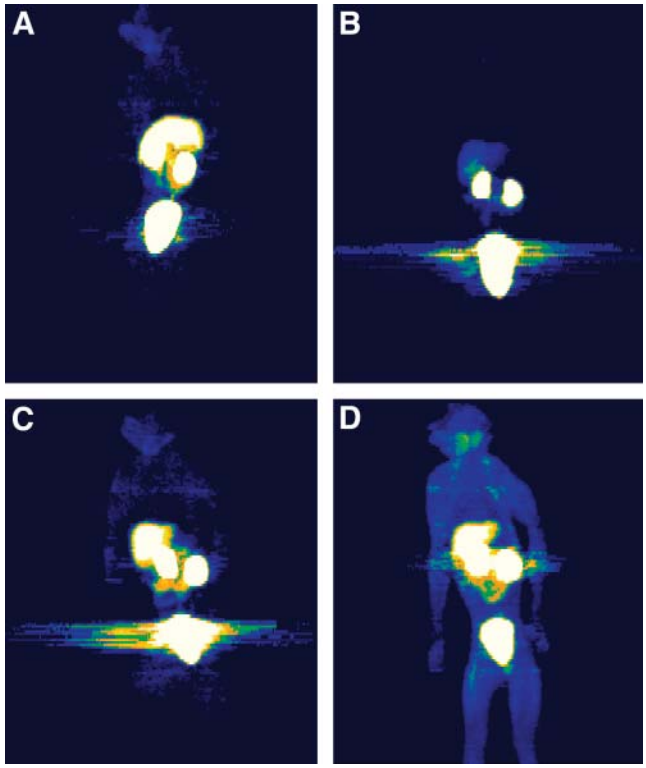

FIGURE 5. MedX (Medical Numerics)-prepared images of PET scans taken before transplantation (A and B) and 6 mo after transplantation (C and D) of hematopoietic stem cells transduced with lentiviral vector containing HSV1-tk for monkeys CJ2R (A and C) and 2RC003 (B and D), with image brightness, contrast, and intensity standardized between the two.

DISCUSSION

Before this study, there had been no pharmacokinetic data, to our knowledge, for ^{76}Br-FBAU in a large-animal model. Also, little work has been done on full-body PET scans in nonhuman primates. Early work has used ^{76}Br to quantitate dopamine receptors (*19*), to radiolabel antibodies for tumor detection (*20,21*), and to evaluate cellular proliferation (*22*). A lipophilic formulation of ^{76}Br-FBAU-dibenzoate has been used as a tracer for brain imaging in rodent studies (*23*) and, recently, as a PET reporter probe for imaging of HSV1-tk gene expression in a murine model of human glioma (*24*). Our study demonstrated that ^{76}Br-FBAU could be used safely in a nonhuman primate model, thus permitting the extension of imaging times from minutes to hours. During this study, the animals remained healthy and showed no abnormal changes in either complete blood counts or serum biochemistry levels, and the animals continue to remain healthy. The mean α- and β-phase half-lives in whole blood for ^{76}Br-FBAU were 2.60 ± 0.70 min and 107.80 ± 31.92 min, with elimination occurring predominantly within the renal and hepatic organs. Future studies that determine α- and β-phase half-lives in a nonhuman primate model can use these baseline pharmacokinetic data for comparison. ^{76}Br-FBAU elimination was biphasic, fitting a 2-compartment model. What is particularly exciting about ^{76}Br is its long terminal half-life (16.2 h), compared with the half-lives of other commonly used radioisotopes, such as ^{18}F (110 min). Normal distribution is altered by the retention of radiotracer by hematopoietic cells expressing viral tk. The longer it takes for the distribution curve to decrease, the greater the amount of radiotracer retained by transduced hematopoietic cells.

The control animals provided data on the normal pharmacokinetic behavior associated with ^{76}Br-FBAU at a specific dose of 74 MBq. Monkey 2RC003, which consistently had the highest level of EGFP expression and HSV1-tk marking throughout the study, was the animal that displayed the greatest change in pharmacokinetic profile (Fig. 3), distribution (Fig. 4), and image resolution (Fig. 5). Figures 1 and 2 compare the EGFP expression in monkeys 2RC003 and CJ2R at 14 mo. EGFP was expressed in all blood cell types

evaluated—that is, granulocytes, lymphocytes, monocytes, platelets, and red blood cells. The level of EGFP expression also remained relatively level throughout the study. It is interesting to note that both Figures 3 and 4 seem to show a trend toward diminished uptake of ^{76}Br-FBAU over time. This trend may be associated with subtle changes in organ function and vascular integrity after total-body irradiation, followed by the repair of this damage with time. For example, glomerulonephropathy is a common sequela to total-body irradiation.

PET image data (Fig. 5) were analyzed for the amount of radioactivity (pixel brightness) retained in the extremities (Fig. 4). As the primary organ for ^{76}Br-FBAU elimination, the urinary bladder was used as the 100% positive standard. We chose the extremities for analysis because these are the areas in which the hematopoietic environment of the long bones (humerus and femur) can be evaluated with least interference from other organs. When the values in the extremities were standardized to those of the urinary bladder to yield a percentage of radioactivities, the percentage of retained radiolabeled substrate (Fig. 4) significantly differed at all time points after transplantation for monkey 2RC003 ($P < 0.00000042$) but not for monkey CJ2R, a finding that correlates with our observation on real-time PCR analysis. This finding also reflected our observation on monitoring EGFP transgene expression using flow cytometry.

CONCLUSION

Noninvasive molecular imaging using PET correlates with real-time PCR analysis and parallels the expression levels observed for EGFP by flow cytometric analysis. The primary problem remaining is the need to improve image resolution so as to better define specific tissue contributions. Nonetheless, the images demonstrated diffuse retention of ^{76}Br-FBAU by the vasculature and spleen. This pilot study clearly demonstrated the potential of this technology in gene therapy for noninvasive tracking of the progeny of cells marked with the tk reporter gene. The data showed high significance in evaluating multiple time points and comparing the findings with a large number of controls. Certainly, larger studies involving more animals will help confirm the significance of these preliminary results, as will improvements in vector design and gene therapy. With further refinement of imaging technology, improvement of gene transfer, improvement of expression at the cellular level, and enhancement of specific molecular uptake of the radioisotope, real-time analysis of gene expression using PET will become possible, allowing better definition of cellular populations within an organ. Amazingly, in this study, the progeny of a small number of cells ($2–3 \times 10^7$ immunoselected CD34$^+$ cells) could be detected effectively using molecular imaging by PET more than 1 y after transplantation. The promise is that future molecular imaging will allow in vivo localization of transduced cells in real time.

ACKNOWLEDGMENTS

This research was supported in part by the Intramural Research Program of the NIH. We thank Dr. Bill Eckelman, Dr. Peter Herscovitch, and Laura Ravasi for their help, guidance, and assistance in developing the model and for suggesting the use of ^{76}Br. We also thank Amanda DeMaster for her assistance in processing the data; Dr. Dong Sung An for review of the manuscript; and the technical, animal management, and veterinary staff of 5 Research Court for their support in performing this project.

REFERENCES

1. Bhaumik S, Gambhir SS. Optical imaging of Renilla luciferase reporter gene expression in living mice. *Proc Natl Acad Sci U S A.* 2002;99:377–382.
2. Michalet X, Pinaud FF, Bentolila LA, et al. Quantum dots for live cells, in vivo imaging, and diagnostics. *Science.* 2005;307:538–544.
3. Shapiro EM, Skrtic S, Sharer K, Hill JM, Dunbar CE, Koretsky AP. MRI detection of single particles for cellular imaging. *Proc Natl Acad Sci U S A.* 2004;101:10901–10906.
4. Yu Y, Annala AJ, Barrio JR, et al. Quantification of target gene expression by imaging reporter gene expression in living animals. *Nat Med.* 2000;6: 933–937.
5. Gambhir SS, Barrio JR, Phelps ME, et al. Imaging adenoviral-directed reporter gene expression in living animals with positron emission tomography. *Proc Natl Acad Sci U S A.* 1999;96:2333–2338.
6. Jacobs A, Tjuvajev JG, Dubrovin M, et al. Positron emission tomography-based imaging of transgene expression mediated by replication-conditional, oncolytic herpes simplex virus type 1 mutant vectors in vivo. *Cancer Res.* 2001;61: 2983–2995.
7. Koehne G, Doubrovin M, Doubrovina E, et al. Serial in vivo imaging of the targeted migration of human HSV-TK-transduced antigen-specific lymphocytes. *Nat Biotechnol.* 2003;21:405–413.
8. Jacobs A, Voges J, Reszka R, et al. Positron-emission tomography of vector-mediated gene expression in gene therapy for gliomas. *Lancet.* 2001;358: 727–729.
9. Gambhir SS, Bauer E, Black ME, et al. A mutant herpes simplex virus type 1 thymidine kinase reporter gene shows improved sensitivity for imaging reporter gene expression with positron emission tomography. *Proc Natl Acad Sci U S A.* 2000;97:2785–2790.
10. Donahue RE, Kuramoto K, Dunbar CE. Sources and methods for obtaining stem and progenitor cells. In: Coligan JE, Bierer BE, Margulies DH, Shevach EM, Strober W, eds. *Current Protocols in Immunology.* Hoboken, NJ: Wiley; 2005:chap 22, section A.
11. Kung SK, Bonifacino A, Metzger ME, Ringpis GE, Donahue RE, Chen IS. Lentiviral vector-transduced dendritic cells induce specific T cell response in a nonhuman primate model. *Hum Gene Ther.* 2005;16:527–532.
12. Sugiyama O, An DS, Kung SP, et al. Lentivirus-mediated gene transfer induces long-term transgene expression of BMP-2 in vitro and new bone formation in vivo. *Mol Ther.* 2005;11:390–398.
13. Black ME, Kokoris MS, Sabo P. Herpes simplex virus-1 thymidine kinase mutants created by semi-random sequence mutagenesis improve prodrug-mediated tumor cell killing. *Cancer Res.* 2001;61:3022–3026.
14. An DS, Morizono K, Li QX, Mao SH, Lu S, Chen IS. An inducible human immunodeficiency virus type 1 (HIV-1) vector which effectively suppresses HIV-1 replication. *J Virol.* 1999;73:7671–7677.
15. Yee JK, Friedmann T, Burns JC. Generation of high-titer pseudotyped retroviral vectors with very broad host range. *Methods Cell Biol.* 1994;43:99–112.
16. Pantuck AJ, Matherly J, Zisman A, et al. Optimizing prostate cancer suicide gene therapy using herpes simplex virus thymidine kinase active site variants. *Hum Gene Ther.* 2002;13:777–789.
17. Szajek LP, Kao CHK, Kiesewetter DO, et al. Semi-remote production of Br-76 and preparation of high specific activity radiobrominated pharmaceuticals for PET studies. *Radiochimica Acta.* 2004;92:291–295.
18. Yamaoka K, Nakagawa T, Uno T. Application of Akaike's information criterion (AIC) in the evaluation of linear pharmacokinetic equations. *J Pharmacokinet Biopharm.* 1978;6:165–175.
19. Maziere B, Loc'h C, Baron JC, et al. In vivo quantitative imaging of dopamine receptors in human brain using positron emission tomography and [^{76}Br]bromospiperone. *Eur J Pharmacol.* 1985;114:267–272.

20. Lovqvist A, Sundin A, Ahlstrom H, Carlsson J, Lundqvist H. ^{76}Br-labeled monoclonal anti-CEA antibodies for radioimmuno positron emission tomography. *Nucl Med Biol.* 1995;22:125–131.
21. Lovqvist A, Sundin A, Roberto A, Ahlstrom H, Carlsson J, Lundqvist H. Comparative PET imaging of experimental tumors with bromine-76-labeled antibodies, fluorine-18-fluorodeoxyglucose and carbon-11-methionine. *J Nucl Med.* 1997;38:1029–1035.
22. Bergstrom M, Lu L, Fasth KJ, et al. In vitro and animal validation of bromine-76-bromodeoxyuridine as a proliferation marker. *J Nucl Med.* 1998;39:1273–1279.
23. Kao CH, Waki A, Sassaman MB, et al. Evaluation of [^{76}Br]FBAU 3′,5′-dibenzoate as a lipophilic prodrug for brain imaging. *Nucl Med Biol.* 2002;29:527–535.
24. Cho SY, Ravasi L, Szajek LP, et al. Evaluation of ^{76}Br-FBAU as a PET reporter probe for HSV1-tk gene expression imaging using mouse models of human glioma. *J Nucl Med.* 2005;46:1923–1930.